

**HARNESSING ‘TIME’ TO ENHANCE MEMORY:
USING CLOSED-LOOP TECHNOLOGY TO FACILITATE OSCILLATORY
SYNCHRONY & SUPPORT COGNITION**

by

Andrew C. Garcia

A thesis submitted to the Faculty of the University of Delaware in partial
fulfillment of the requirements for the degree of Master of Science in Neuroscience

Spring 2019

© 2019
All Rights Reserved

**HARNESSING ‘TIME’ TO ENHANCE MEMORY:
USING CLOSED-LOOP TECHNOLOGY TO FACILITATE OSCILLATORY
SYNCHRONY & SUPPORT COGNITION**

by

Andrew C. Garcia

Approved: _____
Amy L. Griffin, Ph.D.
Professor in charge of thesis on behalf of the Advisory Committee

Approved: _____
Robert F. Simons, Ph.D.
Chair of the Department of Psychological and Brain Science

Approved: _____
John Pelesko, Ph.D.
Interim Dean of the College of Arts and Sciences

Approved: _____
Douglas J. Doren, Ph.D.
Interim Vice Provost for Graduate and Professional Education

ACKNOWLEDGMENTS

I would like to extend my deepest gratitude toward my advisor, Amy Griffin, who continually showed me genuine kindness, patience and understanding, and selfless mentorship – both within and outside of science. We have experienced the ups and downs of science together and from this I have acquired insight and perspective I could not have imagined prior to coming to the University of Delaware. Although we all face trials and tribulations unique to our journey that ultimately shape who we become, I feel fortunate to reflect upon such monumental experiences, like that of graduate school, under the grounded and balanced eye of my advisor Amy. Our discussions together are something I will never forget, but will remain forever appreciative. I would also like to thank my committee members, Tania Roth and Joshua Neunuebel, who graciously accepted to offer their support, guidance, and critique of the current project. The time and consideration you've extended toward me is deeply appreciated and does not go unnoticed. I would also like to extend a very heartfelt thank you to my partner, Lexi Turano. Her unwavering support, rooted in loving care, compassion, and understanding, continuously helps me to keep my gaze focused forward on the summit ahead. Last but not least, I would like to thank my family – my father, David, mother, Laura, and brother, Joseph. The lessons I've learned from them have built the foundation of who I am today, and I could not be more proud to have such strong roots.

Thank you, to each and every one of you. Sincerely.

TABLE OF CONTENTS

LIST OF FIGURES	v
ABSTRACT	ix
Chapter	
1 INTRODUCTION	1
1.1 Theta Oscillations Across Species.....	1
1.2 Hippocampal-Prefrontal Interactions during Spatial Working Memory... 5	
1.3 Utilizing the Theta Rhythm for Learning & Memory	7
2 METHODS	9
2.1 Subjects.....	9
2.2 Surgery	9
2.3 Handling & Training	11
2.4 Behavioral Apparatus & Acquisition Room.....	12
2.5 Data Acquisition, Closed-loop Processing, & Analysis	13
2.6 Experimental Overview	15
3 RESULTS	17
3.1 Hippocampal-Prefrontal Theta Synchrony during Working Memory	17
3.2 Detecting Endogenous Theta Synchrony	19
3.3 Exogenously Inducing Theta Synchrony.....	20
3.4 Driving Theta Rhythmicity in Prefrontal Cortex.....	20
4 DISCUSSION.....	22
FIGURES	27
REFERENCES	37
Appendix	
A ANIMAL PROTOCOL PERMISSION	47

LIST OF FIGURES

- Figure 1 **HPC-mPFC high theta coherence events as rats performed a delayed alternation task on a T-maze.** (A) Since high theta coherence was previously reported to be concentrated at the choice point (red on maze inset), we focused our analysis on times when rats entered the central stem to the time they entered one of the two reward zones (yellow on maze inset). From a total of 28 sessions (4 each from 7 rats), we find the average duration of a high theta coherence event to be 724.28 milliseconds ($n = 29,321$ theta bouts). (B) Left, box plots showing the number of high theta coherence bouts per session (4 sessions per rat) for each of the seven rats. Right, average number of high theta coherence bouts per session across rats (104.71 bouts ± 28.49 sem, $n = 7$ rats), with individual rat averages overlaid as dots. (C) Left, box plots showing the duration of high theta coherence bouts per session (4 sessions per rat) for each of the seven rats. Right, average duration of high theta coherence bouts per session across rats (708.25 ms ± 18.72 sem, $n = 7$ rats), with individual rat averages overlaid as dots. (D) The number of high theta coherence bouts per session did not correlate with the average duration of high theta coherence bouts per session ($p > .05$, $n = 28$ sessions from 7 rats)..... 27

Figure 2 mPFC theta phase precedes HPC theta phase. (A) To understand theta phase relations between HPC and mPFC during high theta coherence states, we filtered for the theta frequency in each region (mPFC - top, magenta; HPC - bottom, black) from their raw LFP traces (grey, mPFC - top and HPC - bottom) and extracted their theta phases (middle, magenta-mPFC, black-HPC). (B) We find that HPC theta phase shortly follows mPFC theta phase during high theta coherence states (mean (red) \pm sem: $105.38^\circ \pm 6.47^\circ$, $n = 28$ sessions from 7 rats). Note the clustering of phase angle differences consistently indicating HPC phase following mPFC phase ($p < .001$ for Rayleigh's test of nonuniformity, $n = 28$ sessions from 7 rats). (C) Using HPC theta troughs as event flags for plotting mPFC LFP in this LFP-triggered average reveals that HPC does shortly follow mPFC (note: red trough (mPFC) slightly shifted to the left of vertical reference line depicting HPC theta troughs (grey)). (D) Inset, quantification of this phase offset using a phase-lag index further reveals the directionality of these phase differences (mean \pm sem: $.59 \pm .05$, $n = 28$ sessions from 7 rats); however, there is no correlation between the magnitude of the phase difference and the calculated phase-lag index (main panel, $p > .05$). 28

Figure 3 Utilizing endogenous HPC-mPFC theta synchrony. (A) Schematic depicting the closed-loop to be used for initiating memory task trials based upon detection of high HPC-mPFC theta coherence states. LFPs will be simultaneously recorded from HPC and mPFC and routed to another computer to analyze for theta coherence, and if high theta coherence is detected, then a TTL pulse will be sent to initiate the opening of an automated door on the T-maze. (B) Top rows, raw LFP traces from mPFC and HPC with filtered theta overlaid showing high theta coherence in blue. Middle rows, coherogram depicts high theta coherence represented via the warmer colors toward the theta range (4-12 Hz), with the line plot showing high coherence specific to the theta frequency range. This example detection of a high theta coherence state would initiate a command to send a TTL pulse that would be used to open a door on the maze and initiate a memory task trial for the rat to perform (bottom left). However, if HPC-mPFC theta coherence remains low and does not exceed the high coherence threshold, then the door will remain closed (bottom right). Bottom middle, the current loop successfully detects high theta coherence states 89% of the time; however, this will likely increase to 100% with supplemental programming of the Hardware Processing Platform (HPP) to be used in tandem with our digital recording system (Digital Lynx, Neuralynx) to fully support low-latency feedback stimulation. ... 29

- Figure 4 **Schematic of the closed-loop for detecting high HPC-mPFC theta coherence in real-time.** Upper left panel on screen depicts mPFC LFP (blue), bottom left panel depicts HPC LFP (magenta), top right panel depicts wideband coherence spectrum, and bottom right depicts coherence specific to the theta frequency band. Note the dynamic tracking of HPC-mPFC theta coherence in the bottom right portion of the screen with green and red signaling high and low levels of theta coherence..... 30
- Figure 5 **Exogenously driving theta activity in mPFC.** (A) Schematic depicting the closed-loop for inducing theta rhythmicity in mPFC via detected theta activity in HPC. First, a viral vector containing Channelrhodopsin is injected into mPFC to transduce neurons with an excitatory opsin. Subsequently, electrodes are placed in HPC and mPFC with an optic fiber positioned over mPFC to activate the transduced neurons with blue light (450 nm). Operation of the closed-loop will record LFP activity from HPC and route it to another computer which will analyze for theta power, and if HPC is in a theta state, then blue light pulses will emitted over mPFC at the HPC theta frequency to facilitate HPC-mPFC theta synchrony. LFP activity from mPFC will be recorded and later analyzed offline. (B) From the time the blue light pulse is emitted, the induced excitation is observed in the LFP with a peak deflection occurring at an 11 millisecond latency (grey lines depict multiple LFP traces from multiple theta stimulation trains overlaid). (C) Top rows, raw LFPs (grey) with filtered theta overlaid (black), with induced theta rhythmicity in mPFC via a 1-second 8-Hz stimulation train (blue). Bottom rows, blue light theta pulses in mPFC increase mPFC theta power, and increase HPC-mPFC theta coherence depicted in the coherogram, with warmer colors indicating higher coherence in the theta frequency range, and in the line plot below depicting theta frequency band-specific coherence..... 31
- Figure 6 **Exogenously inducing theta rhythmicity in mPFC increases HPC-mPFC theta coherence.** (A) Blue light pulses delivered at the theta frequency increases phase coherence between HPC and mPFC in the theta frequency range (5-12 Hz) (pre-stim, grey; post-stim, blue, n = 4 rats). (B) Theta band-specific coherence is higher during blue light stimulation (mean \pm sem: pre: $.59 \pm .01$, post: $.68 \pm .3$; Kolmogorov-Smirnov test, p = .0111, n = 4 rats). (C) Individual coherence plots for each rat for pre- and post-stimulation..... 32

Figure 7	<p>Schematic of inducing theta rhythmicity and increasing HPC-mPFC theta coherence in real-time. Upper left panel on screen depicts mPFC LFP (blue), bottom left panel depicts HPC LFP (magenta), top right panel depicts wideband coherence spectrum, and bottom right depicts coherence specific to the theta frequency band. Note the induced theta rhythm in mPFC (blue) during blue light theta frequency pulsing in the bottom left, and the increase in HPC-mPFC coherence in the bottom right.</p>	33
Figure 8	<p>Theta pulsing in mPFC increases theta-gamma coupling. (A) Heat maps showing higher coupling of gamma amplitude to theta phase in mPFC during blue light stimulation as depicted via warmer colors toward the center of the theta cycle phase range in the post-stim compared to the pre-stim. (B) Quantifying the degree of theta phase-gamma amplitude coupling shows increased coupling with blue light pulsing (pre: $.0023 \pm .00062$, post: $.0033 \pm .00056$; Kolmogorov-Smirnov test, $p > .05$, $n = 4$ rats).</p>	34
Figure 9	<p>Blue light pulsing increases information entropy. Note the change in the probability distributions in the bottom row, as higher entropy indicates the amount of ‘information’ contained in the LFP, as indexed by the probability that an LFP value will fall within a particular voltage bin.</p>	35
Figure 10	<p>Schematic for automated T-maze. A combination of motors and infrared beam detectors will be programmed with an Arduino microcontroller, used in conjunction with an overhead camera for spatial tracking, to interface with the closed-loops to control trial start times and blue light pulsing. A microcontroller board attached to a prototyping board will be used to configure and control input-out relations to what is programmed in the microcontroller. The prototyping board will be designed to interface the microcontroller with the motors and sensors positioned on the maze. Two servo motors will be used to control the doors that will be used to confine the rat to the start box zone on the maze. Three sets of photo beams will be used to detect when the rat has entered specific zones (i.e., left/right reward zones and start box zone). Two stepper motors will be used to dispel liquid reward in the reward zones and each will be powered by a motor driver.</p>	36

ABSTRACT

The theta rhythm (4-12 Hz) in hippocampus (HPC) has been shown to support learning and memory, often by synchronizing with interconnected brain regions to meet task demands. One key brain region with which the HPC synchronizes during spatial working memory is the medial prefrontal cortex (mPFC). Although it has been shown that unsuccessful spatial working memory performance, or manipulations that impair performance, are accompanied by decreased HPC-mPFC theta synchrony, it remains to be determined if harnessing endogenous theta synchrony, or exogenously driving theta synchrony, can be used to facilitate learning or enhance memory ability. To begin to explore these questions, we have designed a brain-machine interface to support closed-loop processes of reiteratively recording and analyzing neural input and conditionally implementing machine interventions. The first experiment uses closed-loop technology to simultaneously record local field potentials (LFPs) from both HPC and mPFC and calculate HPC-mPFC theta coherence. If high theta coherence between these regions is detected, then a command is sent to trigger a door opening which would initiate a memory task trial. The second experiment uses closed-loop technology in conjunction with optogenetics to record LFP activity from HPC, analyze power spectral density, and if HPC theta power is high, send a command to stimulate a laser in mPFC at HPC's theta frequency to facilitate HPC-mPFC theta synchrony. The current project provides foundational proof-of-concept data that our brain-machine interface has the capability to increase the degree to which HPC and mPFC are theta-synchronous. This work provides future studies with the ability to apply this intervention in the context of enhancing learning and memory capabilities in the rodent.

Chapter 1

INTRODUCTION

The theta rhythm is a large amplitude, nearly sinusoidal 4-12 Hz oscillatory pattern readily observed in the hippocampus (HPC), in addition to other regions in the brain. This distinct oscillatory waveform was first recorded from the hippocampus of rabbits in 1938 (Jung & Kornmuller, 1938). A subsequent study in 1954 analyzed recordings from rabbits, cats, and monkeys and identified that this synchronized oscillatory pattern in the HPC co-occurred with desynchronized oscillatory activity in the neocortex particularly during states of alertness and arousal (Green & Arduini, 1954). Since then, the theta rhythm was found to support learning and memory processes such as the development of conditioned reflexes, spatial discrimination learning, inhibitory avoidance learning, and classical conditioning (Graystan et al., 1959; Adey et al., 1960; Landfield et al., 1972; Berry & Thompson, 1978).

1.1 Theta Oscillations Across Species

The appearance of this slow oscillation correlates with a variety of behaviors, including preparatory behaviors, orienting behaviors, exploratory behaviors, locomotive behaviors, and memory-guided behaviors (Buzsaki, 2002). Although the

vast majority of studies on the HPC theta rhythm use rodents, the theta rhythm has been observed in other species including rabbits, gerbils, hamsters, pigs, pigeons, dogs, cats, bats, and primates (Graystan, et al., 1959; Brown, 1968; Macrides, 1975; Forslid et al., 1986; Siegel et al., 2000; Ulanovsky & Moss, 2007; Ulanovsky & Moss, 2013; Jutras et al., 2013; Watrous et al., 2013; Leonard et al., 2015; Aghajan et al, 2017; Bohbot et al., 2017). In contrast to the sustained theta oscillations observed in most species, theta frequency activity observed in bats and primates have been found to occur in short intermittent bouts (Ulanovsky & Moss, 2007; Jutras et al., 2013; Watrous et al., 2013; Leonard et al., 2015; Aghajan et al, 2017; Bohbot et al., 2017).

In bats, theta oscillations tend to occur during immobility, last approximately 1-2 seconds, have a peak frequency between 5-7 Hz, and co-occur with increases in echo call rates (Ulanovsky & Moss, 2007). Although theta modulation of bat HPC neurons was observed during non-locomotive exploratory behaviors, there was a near absence of theta modulation in these neurons during crawling or flight (Ulanovsky & Moss, 2007; Yartsev & Ulanovsky, 2013). Additionally, grid cells in bat entorhinal cortex showed similar spatially-hexagonal firing patterns to those observed in the rodent; however, spiking activity of these bat grid cells existed without continuous theta oscillations unlike those in the rodent (Yartsev et al., 2011; Brandon et al., 2011). It is postulated that this lack of observed theta rhythmicity in bat neurons is attributable to a lack of theta-frequency membrane resonance, low firing rates making it difficult to adequately examine and detect theta rhythmicity, or a combination of the two (Barry et al., 2012; Heys et al., 2013; Climer et al., 2015). Interestingly, it was

recently found that bat HPC neurons phase-lock to non-rhythmic fluctuations in the 1-20 Hz frequency range in the field potential, with some neurons exhibiting phase-precession, whereby spikes advance to earlier phases of this 1-20 Hz waveform as the bat progressed through that neuron's place field (Eliav et al., 2017).

Theta bouts in non-human primates tend to last approximately 3-10 cycles in duration, have a peak frequency between 8-11 Hz, and tend to initiate a theta phase reset upon visual saccade (Jutras et al., 2013; Leonard et al., 2015; Leonard & Hoffman, 2017). Contrary to bats, neurons in monkey entorhinal cortex tend to show theta modulation (Killian et al., 2012). Recent studies investigating human theta activity found that in addition to saccade-modulated theta activity, real-world ambulatory movement induced theta activity with a peak frequency between 6-10 Hz, compared to lower frequencies often observed during virtual navigation (Hoffman et al., 2013; Watrous et al., 2013; Bohbot et al., 2016; Aghajan et al., 2017). These movement-related theta bouts tend to occur for durations around 400 milliseconds and were found to increase with speed, similar to speed-modulated theta activity observed in rodents (Aghajan et al., 2017). Another human study, albeit using virtual navigation, found higher frequency theta oscillations in the human posterior HPC (~8 Hz) compared to the anterior HPC (~3 Hz) (Goyal et al., 2018). This is similar to that observed in the rat where dorsal HPC, homologous to human posterior HPC, tends to exhibit a higher peak theta frequency than ventral HPC, homologous to human anterior HPC (Schmidt et al., 2013). One question that remains is if subtle differences in theta activity still support a common function amongst different species.

The common substrate for species-specific theta activity may lie within how each animal acquires information about the environment. This notion would be supported by echo call-modulated theta activity in bats, saccade-modulated theta activity in primates, and movement-modulated theta activity in rodents and humans, whereby it can be predicted that non-human primate theta would also be modulated by movement. Theta activity can also be modulated by the degree to which an animal is attentive to the environment as theta activity in the cat increases during active visual search or prey fixation, theta activity in the rat increases during tail pinch and rearing, and saccade-induced theta phase reset in non-human primates was found to predict memory performance (Winson, 1972; Robinson et al., 1980; Jutras et al., 2013). Such attention-related theta modulation is compatible with the sensorimotor integration theory of theta oscillations, which posits that the theta frequency may serve to coordinate and update neural representations for motor performance in relation to changes in the external sensory world (Bland, 1986; Bland & Oddie, 2001). As an animal acquires sensory data about the external environment via their primary modality, motor control of sensory systems continuously initiates a chain of neural activity involving numerous interconnected brain areas (Amit et al., 2017).

As rats performed a whisker-mediated texture discrimination task, it was found that whisking, which occurs at the theta frequency, synchronizes with HPC theta activity to entrain neurons in the barrel cortex, the region in which whisk-related signals enter the neocortex, to support successful task performance (Grion et al., 2016). In another study in which monkeys performed a visuospatial attention task,

theta and gamma frequencies were found to support bottom-up processing streams in visual areas (Bastos et al., 2015). This frequency band-specific stream of information flow is of interest as theta-based information flow has been observed in the rat HPC-to-lateral septum pathway and the entorhinal-HPC circuit, amongst other interregional pairs (Schomburg et al, 2014; Tingley & Buzsaki, 2018).

Although the theta rhythm has not been found to modulate neuronal spiking activity in bats, it is possible that the non-theta modulated neurons were not relevant for that particular behavior or function and that theta frequency-synchronization may be evident when interconnected brain areas need to share or coordinate neural representations. However, it may also be that some species rely more on oscillations to support neural synchrony and temporal organization such as the crucial role of the medial septum in rodents, whereas other species such as primates and bats may have alternative mechanisms to support spike organization and neuronal synchrony. Future studies can begin to address these questions by developing tasks that would be comparable in nature for rodents, bats, and primates where multisite recordings in each of these species might further tease apart inherent physiological differences in the role of oscillatory activity in neuronal synchronization and behavior.

1.2 Hippocampal-Prefrontal Interactions during Spatial Working Memory

The theta rhythm is known to play an important role in spatial working memory, which requires encoding goal-relevant information, temporarily retaining

that mnemonic information, and then retrieving that memory to guide subsequent decision making. In rodents, spatial working memory is supported not only by the functional integrity of the HPC, but also by functional interactions with the mPFC (Floresco et al., 1997; Churchwell et al., 2010). Closer examination of the nature of HPC-mPFC interactions has identified oscillatory synchrony as the mechanism for their spatial working memory-supportive relations, particularly via the theta frequency (Jones & Wilson, 2005; Benchenane et al., 2010; Hyman et al., 2010; Colgin, 2011; Gordon, 2011; O'Neill et al., 2013; Myroshnychenko et al., 2017).

Theta-based synchrony between two brain regions can occur via a variety of different means and configurations, with one commonly observed measure of theta synchrony being phase coherence. Phase coherence measures the degree to which two simultaneously recorded LFPs show a consistent phase-to-phase relationship for a specific frequency range over time, such that their peaks and troughs tend to rise and fall together. The electrical activity recorded from the LFP represents the extracellularly-recorded net flow of transmembrane currents, primarily from synaptic activity, from large populations of neurons in the vicinity of the recording electrode (Buzsaki et al., 2012). Although it has been extensively shown that successful spatial working memory performance is accompanied by strong HPC-mPFC theta coherence, it remained to be determined if, and how, perturbing spatial working memory faculties might affect HPC-mPFC theta synchrony.

To further understand the relationship between spatial working memory abilities and HPC-mPFC synchrony, a region shown to be critical for spatial working

memory performance and is reciprocally connected with both HPC and mPFC, the nucleus reuniens, was pharmacologically inactivated while recording from both HPC and mPFC. Inactivation of the nucleus reuniens during a delayed alternation task not only impaired performance on this task but also led to a dramatic reduction in the degree to which HPC and mPFC synchronized, particularly at the theta frequency (Hallock et al., 2016). In addition to decreasing theta phase coherence, inactivating nucleus reuniens also decreased coupling between mPFC gamma amplitude and HPC theta phase and coupling between spike times from mPFC neurons and HPC theta phase, both of which have been observed during successful spatial working memory performance (Siapas et al., 2005; Jones & Wilson, 2005; Benchenane et al., 2010; Hyman et al., 2010; Hallock et al., 2016; Tamura et al., 2017). Collectively, these studies show that HPC-mPFC interactions relevant to spatial working memory-guided behavior are supported by theta-based oscillatory activity, presumably by coordinating afferent and efferent signals within this circuit to selectively transmit behaviorally-relevant information (Buzsáki, 2006; Fell & Axmacher, 2011; Saalman, 2014).

1.3 Utilizing the Theta Rhythm for Learning & Memory

Another important question remains, is it possible to enhance memory performance by facilitating theta synchrony? A similar question was approached by designing a brain-machine interface programmed to assess the degree to which spontaneous theta oscillations were present in HPC, and initiate trials contingent upon

theta presence. Not only did the theta-triggered animals learn faster than the nontheta-triggered animals, in both delay and trace eye blink conditioning paradigms, but this closed-loop approach also enhanced the degree to which neurons in HPC represented salient task events reflected in their firing rates (Seager et al., 2002; Griffin et al., 2004).

To model this approach and modify it for spatial working memory processes, we have designed a similar closed-loop approach that will 1) assess the degree to which HPC and mPFC show spontaneous theta synchrony and initiate trials based upon high theta coherence, and 2) drive theta-rhythmic activity in mPFC to synchronize with spontaneously occurring theta oscillations in HPC using optogenetic stimulation. These approaches are designed to facilitate the rate of learning, as well as test to see if memory performance can be enhanced by increasing the memory demand during induced theta-synchrony. This thesis will culminate in the completion of pilot testing our closed-loop brain-machine interfaces and the construction of the automated maze whose functions will be programmed to operate under the control of the closed-loop data processing streams. Broad implications for closed-loop approaches such as this include development, refinement, and application of neurotherapeutic interventions geared toward rescuing deficits in circuit-level synchrony observed in psychiatric disorders and disease states such as Schizophrenia and Alzheimer's disease (Sigurdsson et al., 2010; Kitchigina, 2018).

Chapter 2

METHODS

2.1 Subjects

Subjects were adult (>90 days old) male Long-Evans rats weighing between 300 and 600 grams at the time of surgery. Four rats were used for endogenous theta detection and exogenous theta induction, while seven rats were used for analyzing previously-recorded data from a delayed alternation task. Each rat was placed on mild food restriction (~4 food pellets per day) to keep each rat at ~90% of his *ad libitum* body weight. All rats were housed individually in a temperature- and humidity-controlled colony room with a 12-hour light/dark cycle with all behavioral testing and data acquisition occurring during the light cycle. All procedures were carried out in accordance with the University of Delaware Institutional Animal Care and Use Committee.

2.2 Surgery

During surgery, an injection of atropine was given and the rat will was placed inside a Plexiglass flow box where anesthetization was initiated using isoflurane gas (3.5% in oxygen) and maintained on 1-2%. Lubricant ophthalmic ointment was

applied to the eyes, the head was shaved, and the subject was head-fixed into a stereotaxic instrument (Kopf Instruments). Prior to incision, lidocaine was injected subcutaneously into the scalp. The head was leveled and bregma coordinates were identified. Six small bone screws (Fine Science Tools) were fitted into burr holes made into the skull with a stereotaxically mounted drill (Foredom Electric Co.). Dental acrylic (Lang Dental) was applied to anchor the screws to the skull. Craniotomies were made to target medial prefrontal cortex (PL/IL) and hippocampus (dorsal CA1).

Two surgeries were required to accommodate both Aims 1 and 2. During the first surgery, a Channelrhodopsin virus (pAAV-hSyn-hChR2(H134R)-EYFP) was injected at four locations in the PL/IL area (3.2 mm anterior to bregma, 0.5 mm from the midline, 4.6 and 2.7 mm from brain surface). Three weeks later, the second surgery was carried out which consisted of implanting electrodes into the HPC and mPFC, while additionally positioning an optic fiber over mPFC. This temporal interval, in addition to the week of post-surgery recovery provided adequate time for the virus to transduce neurons at the injection sites. For recording LFP activity, circular holes were drilled above HPC (4.2 mm posterior to bregma, 2.1 mm from the midline) with gross electrodes positioned 2.4 mm from brain surface, and above mPFC (3.7 mm anterior to bregma, 0.6 mm from the midline) with gross electrodes positioned 2.9 mm from brain surface. The optic fiber was positioned over medial prefrontal cortex (PL/IL) 2.1 mm from brain surface.

Electronic interface boards were attached to a ground screw (a self-tapping bone screw with a piece of wire soldered to it), which was fitted into a small burr hole directly above the lambda skull suture. Craniotomies around the implants were sealed with Kwik-Cast (World Precision Instruments), and the entire implant was secured to the skull with dental acrylic. A subcutaneous injection of flunixin (Banamine; 2.5 mg/kg) was given and children's ibuprofen (30 mg/kg) was placed in the drinking water for 2-3 days after surgery. After the surgery, monitoring occurred daily and at least five days of rest was allowed for post-surgery recovery.

2.3 Handling & Training

Before data acquisition, handling and pre-training procedures were implemented (Hallock & Griffin, 2013; Hallock et al., 2013a; Hallock et al., 2013b). Handling occurred for five days outside of the acquisition room for a minimum of five minutes each day to acclimate to human contact and introduce to reward foods, which was given at the home cage following each handling period. Following handling, "goal zone" training sessions began, which limited exploration to the reward zones at the end of the goal arms where free access to reward foods was given. After a minimum of two days of "goal zone" training, "forced run" trials began which consisted of behavioral shaping such that they learned to run down the central stem of the maze from the start box pedestal and turn into a pre-determined goal arm according to a pseudorandom sequence (Fellows, 1967). Criterion was said to have

been reached upon two successful sessions of running down and eating the reward across two consecutive days.

2.4 Behavioral Apparatus & Acquisition Room

The maze used was a black, wooden T-maze with 6-cm high walls consisting of a central stem (117 x 9 cm), a perpendicular choice point corridor (106 x 9 cm), two goal arms (38 x 9 cm), two return arms (120 x 9 cm), and a circular waiting arena (37 cm in diameter, attached to a wooden bar stool) which was used in conjunction with a black wooden barrier (30 x 30 cm) to confine rats to this area during intertrial intervals. The T-maze was located in a room that was completely surrounded by black curtains with several visual cues attached to them (i.e., blue square, red vertical stripes, green circle, etc.). The room was dimly illuminated by a compact fluorescent bulb. Before and after recording sessions, rats were placed in a black cotton-lined plastic enclosure (37 cm in diameter) placed in the corner of the room.

Subsequent to data acquisition and analysis, an automated T-maze will be constructed for future behavioral testing using temporally-specific initiation of task trials based upon the real-time detection and analysis of oscillatory activity during the continuous and delayed versions of an alternation task on a T-maze (Fig 10). A microcontroller board (Arduino Mega 2560) will be attached to a prototyping board (Keyestudio Mega Protoshield V3) that will be used to configure and control input-out relations to what is programmed in the microcontroller. The prototyping board will be designed to interface the Arduino with the motors and sensors positioned on the maze.

Two servo motors (A0090) will be used to control the doors that will be used to confine the rat to the start box zone on the maze. Three sets of photo beams (GP1A57HRJ00F) will be used to detect when the rat has entered specific zones (i.e., left/right reward zones and start box zone). Two stepper motors (Mercury motor, SM-42BYG011-25 1812010) will be used to dispel liquid reward in the reward zones and each will be powered by a motor driver (H-bridge 1A). Voltage regulators, resistors, electrolyte decoupling capacitors, diode rectifiers, jumper wires, ribbon cable, and pin housings will be used to assemble the circuit.

2.5 Data Acquisition, Closed-loop Processing, & Analysis

For data acquisition, neural recordings of LFPs were amplified, band-pass filtered between 1 and 2K Hz, and digitized at 2 kHz using a 64-channel recording system (Digital Lynx SX; Neuralynx) and Cheetah software (Neuralynx). LFP signals were recorded with the active electrode referenced directly to a skull screw implanted above the cerebellum. The position of the animal was identified by LEDs mounted on the headstage, which was recorded by an overhead video camera digitized at 30 Hz.

For Aim 1, the closed-loop simultaneously acquired LFPs from HPC and mPFC and continuously shared these signals with another computer that carries the programming platform MATLAB (MathWorks). This interfacing configuration was supported by the application programming interface Netcom (Neuralynx). At the 'MATLAB computer', the LFPs were analyzed using functions from the Chronux toolbox (Mitra & Bokil, 2008) or custom scripts and functions. Coherence, the degree

to which two oscillations show a temporally-consistent angular relationship, was computed using the multi-taper method. If the magnitude of theta coherence exceeded a threshold, then the MATLAB computer sent a command to the acquisition computer to initiate a TTL pulse which will be used to trigger a door opening allowing the rat to initiate a trial (Fig. 3 & 4). The efficacy of high theta coherence-pulse triggering in Aim 1 was assessed by analyzing the proportion of times a ‘door trigger’ pulse was emitted following a high HPC-mPFC theta coherence state.

For Aim 2, the closed loop was developed to record LFP from HPC and share it with the interfacing MATLAB computer. This computer then decomposed the LFP and ran a power spectral density analysis. If the peak power in the broadband (1-50 Hz) power spectrum resided in the theta frequency range, TTL pulses were sent to the acquisition computer to initiate blue light pulses (450 nm) at HPC’s theta frequency. However, due to current limitations on processing speed, an 8-Hz theta frequency pulsing protocol configured internally was implemented via a laser emitting diode box (Doric). Additional programming specific to the Hardware Processing Platform (HPP) used in tandem with our digital recording system (Digital Lynx, NeuroLynx) will enable us with the low-latency feedback capabilities necessary to induce theta rhythmicity in mPFC at the same theta frequency recorded in HPC (Fig. 5 & 7). Phase coherence pre-stimulation was compared against phase coherence post-stimulation.

LFP data previously recorded from HPC and mPFC during the performance of a DA task was used to identify the frequency of high-coherence bouts, the duration of these bouts, and the phase offset between theta oscillations in HPC and mPFC during

these bouts. Identifying the direction of theta phase angle offsets between these two structures during cognition is particularly important as direction-specific synchrony has been observed during distinct components of working memory such as encoding, maintenance, and retrieval (Spellman et al., 2015; Place et al., 2016; Hallock et al., 2016; Bolkan et al., 2017; Myroshenchenko et al., 2017). Moreover, understanding these dynamics will be crucial to initiating blue light stimulation pulses in mPFC at optimal temporal offsets relative to HPC theta phase in attempts to mimic and support neuronal processes underlying cognition rather than perturb them. Furthermore, attempts to emulate naturally-occurring synchrony in the brain, rather than inducing synchrony without consideration of how such manipulations can affect task-relevant neuronal processes, will better adhere to ordinally-precise phase relations and presumably directionally-sensitive streams of information underlying successful spatial working memory processes.

2.6 Experimental Overview

This experiment aimed to develop a brain-machine interface that would support closed-loop processes geared toward enhancing memory function. This first closed-loop was designed to simultaneously record LFPs from HPC and mPFC, analyze for theta coherency, and if high theta coherence is detected, send a command to trigger a door opening which would initiate a memory task trial. The second closed-loop was designed to be used in conjunction with optogenetics to record LFP activity from HPC, analyze power spectral density, and if HPC theta power is high, send a

command to stimulate a laser in mPFC at HPC's theta frequency to facilitate HPC-mPFC theta synchrony. The guided premise for this project was that although it has been shown that unsuccessful spatial working memory performance, or manipulations that impair performance, are accompanied by decreased HPC-mPFC theta synchrony, it remained to be determined if harnessing endogenous theta synchrony, or exogenously driving theta synchrony, can be used to facilitate learning and enhance memory ability.

Chapter 3

RESULTS

3.1 Hippocampal-Prefrontal Theta Synchrony during Working Memory

A previous study from our laboratory showed that HPC-mPFC theta coherence increases selectively at the T-maze choice point during a delayed spatial alternation working memory task (Hallock et al., 2016). To examine this further, we sought to identify how frequently these moments of high theta coherence occurred and how long they lasted. We defined ‘high theta coherence’ as times in which HPC-mPFC theta coherence was greater than or equal to 0.6 (on a scale from 0 to 1) for at least 500 milliseconds. This coherence threshold was selected based upon findings showing HPC-mPFC theta coherence levels greater than or equal to 0.6 during successful performance of a DA task (Hallock et al., 2016). The duration threshold was set so that there will be at least 2-3 full theta cycles to allow for adequate analysis of theta coherence (Cohen, 2014).

Although it was previously demonstrated that HPC-mPFC theta coherence is highest at the choice point (Hallock et al., 2016), we did not restrict our analyses to that specific portion of the maze but instead analyzed LFP activity beginning when the

rat entered the central stem of the maze until when the rat reached a reward zone. This was done to allow identification of the beginning and end of high theta coherence moments as these may potentially be missed if analysis is restricted to the T-junction. We find that moments of high theta coherence tend to occur in a tight cluster of high theta coherence ‘bouts’ centered around the choice point rather than being purely sustained coherent activity. In a delayed alternation session of 18 trials, these high theta coherence bouts occurred an average of 104.71 ± 28.49 times with an average duration of 708.25 ± 18.72 milliseconds (Fig. 1, $n = 7$ rats). Although we did not identify longer intervals of high theta coherence as predicted, it is possible that moments of high theta coherence are actually more sustained than observed here and that subtle variability in the magnitude of coherence within each bout transiently fell below the applied threshold.

To better understand theta phase relations between HPC and mPFC theta waves during moments of high theta coherence at the choice point, we analyzed the phase offset between HPC and mPFC theta activity (Fig. 2A). We find the angular offset between theta phase in HPC and theta phase in mPFC at choice point to be $105.38^\circ \pm 6.47^\circ$, with HPC theta phase shortly following mPFC theta phase (Fig. 2B and 2C, $n = 28$ sessions from 7 rats). Rayleigh’s test of nonuniformity was used to test the null hypothesis that phase offsets between HPC and mPFC are uniformly distributed across the theta cycle’s phase range and revealed that phase offsets were nonuniformly distributed and instead clustered at approximately one quarter cycle offset ($p < .001$, $n = 28$ sessions from 7 rats, $z = 19.61$). To quantify the consistency of

this phase offset, we calculated a phase-lag index which measures the extent to which a distribution of phase angle differences is distributed toward positive or negative values (Cohen, 2014). Across rats, and on a scale from 0 to 1, we find an average phase-lag index of 0.59 ± 0.05 ($n = 28$ sessions from 7 rats) indicating a consistent angular offset between theta phase in mPFC and theta phase in HPC during high theta coherence moments at the choice point (Fig. 2D).

3.2 Detecting Endogenous Theta Synchrony

To assess the efficacy of the closed-loop that was designed to detect moments of high HPC-mPFC theta coherence and trigger a ‘door opening’ via a TTL pulse, we calculated the proportion of times a TTL pulse was emitted following detection of a high HPC-mPFC theta coherence state compared to all high HPC-mPFC theta coherence states subsequently identified offline. We find that on average the closed-loop successfully detects a high theta coherence state and emits a TTL pulse 89% of the time (Fig. 3, $n = 4$ rats). We believe that this current hit rate is likely due to current limitations on processing speed and that detection success will increase with additional programming specific to the Hardware Processing Platform (HPP) used in tandem with our digital recording system (Digital Lynx, NeuraLynx) to support low-latency feedback stimulation experiments.

3.3 Exogenously Inducing Theta Synchrony

To identify if optogenetically driving theta rhythmicity in mPFC increases theta coherence between HPC and mPFC, we compared theta coherence before blue light stimulation and during blue light stimulation, as blue light stimulation (450 Hz) would excite neurons in mPFC previously transduced with the ChR2 viral vector. Due to the processing speed limitations described above, we initiated an 8-Hz theta frequency pulsing protocol configured internally and implemented via a laser emitting diode box (Doric), and restricted analysis to times when HPC was in a theta state. First, we find that optogenetic activation of mPFC neurons induces a deflection in the LFP at a latency of 11 milliseconds (Fig. 5) and that delivery of theta frequency blue light pulses in mPFC increases theta coherence between HPC and mPFC (theta coherence: pre ($0.60 \pm .01$), post ($0.68 \pm .03$); $n = 4$ rats; Fig. 5). A Kolmogorov-Smirnov test identified that coherence between the pre- and post-stimulation conditions were significantly different ($p = .0111$, $n = 4$ rats).

3.4 Driving Theta Rhythmicity in Prefrontal Cortex

Next, we examined if, and how, optogenetically driving theta rhythmicity in mPFC affected cross-frequency coupling between theta phase and gamma amplitude, which is indexed by observing the degree to which gamma power is restricted to a

particular phase of the theta cycle. Theta-gamma coupling is a multiplexed oscillatory configuration believed to organize neuronal activity within and across brain areas to support memory (Lisman & Jensen, 2013). We also examined the degree to which optogenetically driving theta activity in mPFC affected information entropy. Entropy is a measure used to quantify the amount of ‘information’ contained in a variable, as indicated by the degree of ‘uncertainty’ in the probability of that variable’s value, with higher entropy indicating higher information (Shannon, 1948). We find that inducing theta rhythms in mPFC increases theta phase-gamma amplitude coupling (Fig. 8; modulation index: pre (0.0023 ± 0.00062), post (0.0033 ± 0.00056); $n = 4$ rats). A Kolmogorov-Smirnov test did not identify these distributions to be significantly different ($p > .05$); however, this may currently be due to the small sample size as three out of the four rats show a trend in this direction. We also find that driving theta in mPFC increases the amount of entropy in mPFC’s LFP (Fig. 9). Together, these findings show that optogenetically inducing theta rhythms in mPFC holds the potential to mimic, bolster, and potentially enhance neuronal processing capabilities.

Chapter 4

DISCUSSION

Here we contribute to the line of research investigating how theta oscillatory activity supports memory by developing a closed-loop system designed to synchronize hippocampal-prefrontal theta coherence states with memory-demanding task epochs. This work builds upon previous studies using brain machine interfaces to enhance memory by timing task trials with theta states in rats (Seager et al., 2002; Griffin et al., 2004) and humans (Burke et al., 2015), by utilizing times in which disparate brain areas synchronize their theta states in both naturally-occurring settings and also by artificial induction.

We show that moments of high HPC-mPFC theta coherence as rats perform a delayed alternation task tend to occur in bouts and that the phase of HPC theta follows the phase of mPFC theta by approximately one \sim quarter cycle. Identifying the angular offset between theta phases in HPC and mPFC is important for appropriately modeling naturally-occurring theta coherence in the brain and adhering to the endogenous structure of interregional phase-phase relations. The dynamic nature of theta-based functional connectivity was elegantly characterized in a context-guided memory task where the directionality of theta synchrony between HPC and mPFC switched from a HPC-to-mPFC flow during entry into a spatial context to a mPFC-to-HPC flow during

object sampling (Place et al., 2016). A similar mPFC-to-HPC theta directionality was observed in a different memory-based experiment on a plus maze showing that mPFC activity preceded and predicted activity in HPC, putatively biasing HPC to retrieve distinct representations and thus preventing interfering representations and unsuccessful performance (Guise & Shapiro, 2017). Maintaining endogenous phase-phase relations such as those observed in naturally successful performance of a memory task is important for supporting, and not impeding, distinct and temporally-organized streams of information flow during specific components of memory processing.

In addition to showing that inducing theta rhythmicity in mPFC can increase synchrony with HPC, we also show that this pulsing can affect local neuronal processes in mPFC as assessed by the increase in phase-amplitude coupling and information entropy which is important for successful decision-making (Hallock et al., 2016; Tamura et al., 2017). Although single neuron activity was not recorded in these rats, we predict that optogenetic induction of theta rhythmicity in mPFC will entrain single neuron spike times, a commonly observed correlate of successful spatial working memory-guided behavior (Siapas et al., 2005; Jones & Wilson, 2005; Benchenane et al., 2010; Hyman et al., 2010; Hallock et al., 2016; Tamura et al., 2017).

Here we have provided proof-of-concept data showing that optogenetics used in conjunction with electrophysiology and programming platforms can be used to manipulate systems-level oscillatory coordination. However, the parameters of such

neural manipulation will still require careful titration and understanding when attempting to delicately and precisely intervene with cognition and behavior. One initial question that arises when attempting to apply this technology as rats perform a memory-guided task is how will optogenetically activating transduced neurons to drive local theta rhythmicity and interregional theta synchrony affect the mnemonic representations currently supported by active cell assemblies. If the pulse is rather brief, such quick stimulation may not be deleterious to memory-related neuronal activity and neurons may be able to compensate and continue memory-supportive activities. Moreover, this may potentially also recruit and coordinate spiking activity from additional neurons thus increasing the signal-to-noise ratio. Alternatively, it is possible that artificially inducing theta rhythmicity may perturb the natural organization of ongoing neural activity relevant to the task by decreasing the signal-to-noise ratio via recruitment of neurons not currently participating in or relevant to task-related activities. This may unintentionally be caused by stimulation of the excitatory opsin Channelrhodopsin which may induce an oscillatory 'phase reset', thus affecting transmembrane currents across the population and ultimately altering the excitability of task-relevant and task-irrelevant neurons.

However, two approaches can be implemented to circumvent or mitigate these detrimental possibilities. One approach, that is currently underway, is to concurrently identify HPC peaks and troughs so that blue light theta pulses can be initiated in mPFC at phase offsets optimal to theta coherence and successful working memory performance as identified here during the performed of a delayed alternation task.

Another approach that can be used in tandem, is to selectively target and transduce inhibitory interneurons as to leave pyramidal neurons unaffected by blue light stimulation. Although highly-selective optogenetic viral vectors such as these have not been as readily available for rats compared to mice, increased research and development have begun to create such vectors geared toward animals other than mice, ultimately bringing research closer to rat-focused optogenetic manipulation experiments (Dimidschstein et al., 2017). While it is possible, and likely, that driving theta rhythmicity via inhibitory interneurons will indirectly affect pyramidal neuron activity representing mnemonic- or task-related content, this will be drastically minimal compared to directly activating these neurons with blue light. Moreover, inducing theta rhythmicity via interneurons will better model naturally-occurring oscillatory activity and thus lead to a better biology-modeled intervention.

The current work described here provides a strong foundation to utilize closed-loop systems to harness interregional theta synchrony and boost memory performance. We have begun to expand on previous work on the hippocampal theta rhythm and memory by taking a systems-level approach and including a functionally-dependent partner, the medial prefrontal cortex. This is of particular importance as a vast majority of studies in behavioral neuroscience show that although certain brain regions may be necessary for a particular function, it is rather their ability to process inputs from or modify outputs to interconnected brain areas in a dynamic circuit-level cooperation that ultimately supports cognition and behavior. Numerous studies on HPC-mPFC interactions have shown us that interactions in the theta frequency support

memory function. Here we take one step closer toward furthering our understanding of hippocampal-prefrontal interactions by implementing a closed-loop system to identify the causal nature of their theta-based relations in regard to memories supporting decisions.

FIGURES

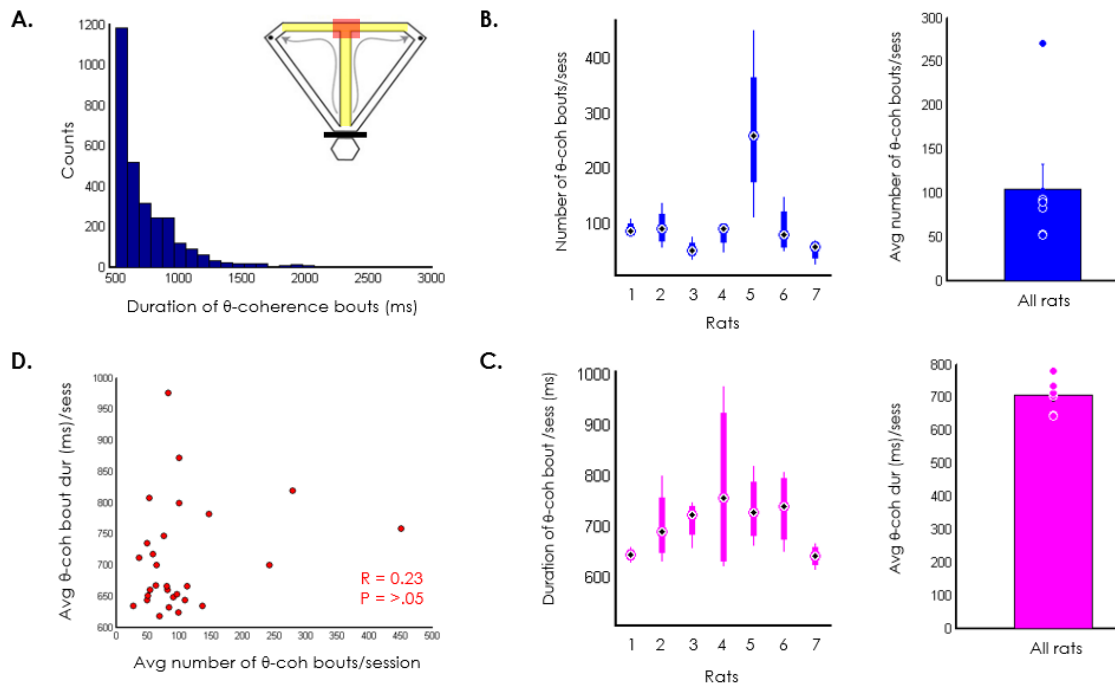


Figure 1 **HPC-mPFC high theta coherence events as rats performed a delayed alternation task on a T-maze.** (A) Since high theta coherence was previously reported to be concentrated at the choice point (red on maze inset), we focused our analysis on times when rats entered the central stem to the time they entered one of the two reward zones (yellow on maze inset). From a total of 28 sessions (4 each from 7 rats), we find the average duration of a high theta coherence event to be 724.28 milliseconds ($n = 29,321$ theta bouts). (B) Left, box plots showing the number of high theta coherence bouts per session (4 sessions per rat) for each of the seven rats. Right, average number of high theta coherence bouts per session across rats ($104.71 \text{ bouts} \pm 28.49 \text{ sem}$, $n = 7$ rats), with individual rat averages overlaid as dots. (C) Left, box plots showing the duration of high theta coherence bouts per session (4 sessions per rat) for each of the seven rats. Right, average duration of high theta coherence bouts per session across rats ($708.25 \text{ ms} \pm 18.72 \text{ sem}$, $n = 7$ rats), with individual rat averages overlaid as dots. (D) The number of high theta coherence bouts per session did not correlate with the average duration of high theta coherence bouts per session ($p > .05$, $n = 28$ sessions from 7 rats).

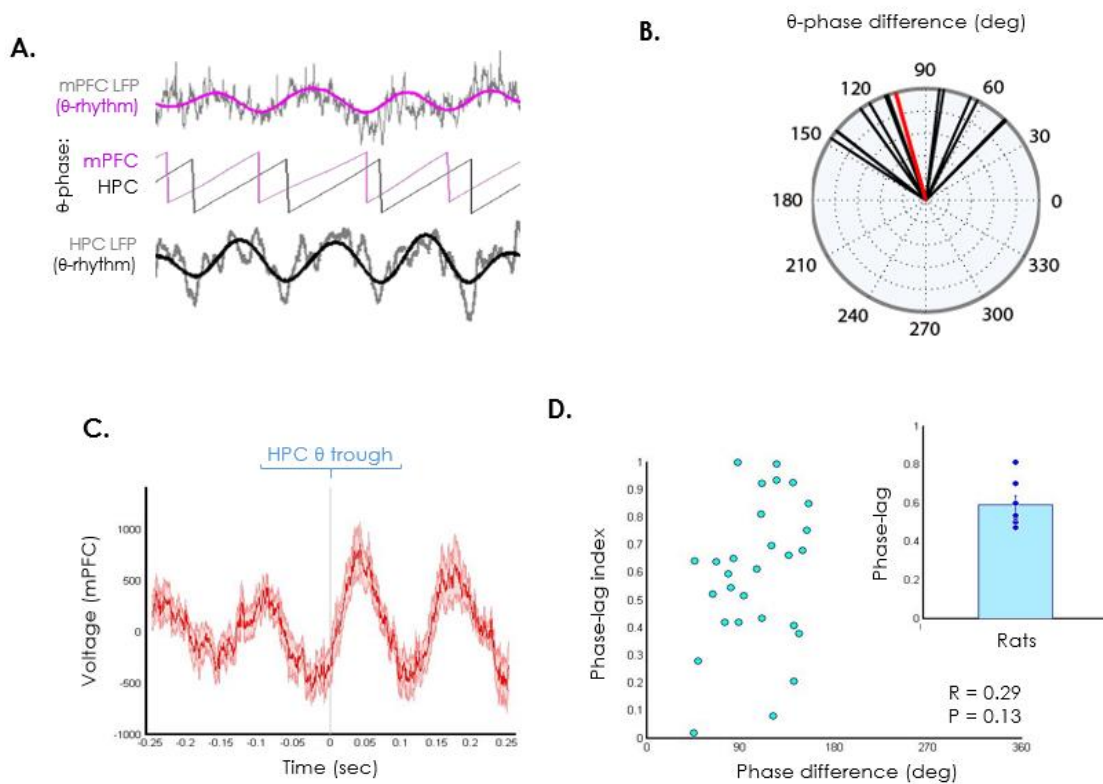


Figure 2 **mPFC theta phase precedes HPC theta phase.** (A) To understand theta phase relations between HPC and mPFC during high theta coherence states, we filtered for the theta frequency in each region (mPFC - top, magenta; HPC - bottom, black) from their raw LFP traces (grey, mPFC - top and HPC - bottom) and extracted their theta phases (middle, magenta-mPFC, black-HPC). (B) We find that HPC theta phase shortly follows mPFC theta phase during high theta coherence states (mean (red) \pm sem: $105.38^\circ \pm 6.47^\circ$, $n = 28$ sessions from 7 rats). Note the clustering of phase angle differences consistently indicating HPC phase following mPFC phase ($p < .001$ for Rayleigh's test of nonuniformity, $n = 28$ sessions from 7 rats). (C) Using HPC theta troughs as event flags for plotting mPFC LFP in this LFP-triggered average reveals that HPC does shortly follow mPFC (note: red trough (mPFC) slightly shifted to the left of vertical reference line depicting HPC theta troughs (grey)). (D) Inset, quantification of this phase offset using a phase-lag index further reveals the directionality of these phase differences (mean \pm sem: $.59 \pm .05$, $n = 28$ sessions from 7 rats); however, there is no correlation between the magnitude of the phase difference and the calculated phase-lag index (main panel, $p > .05$).

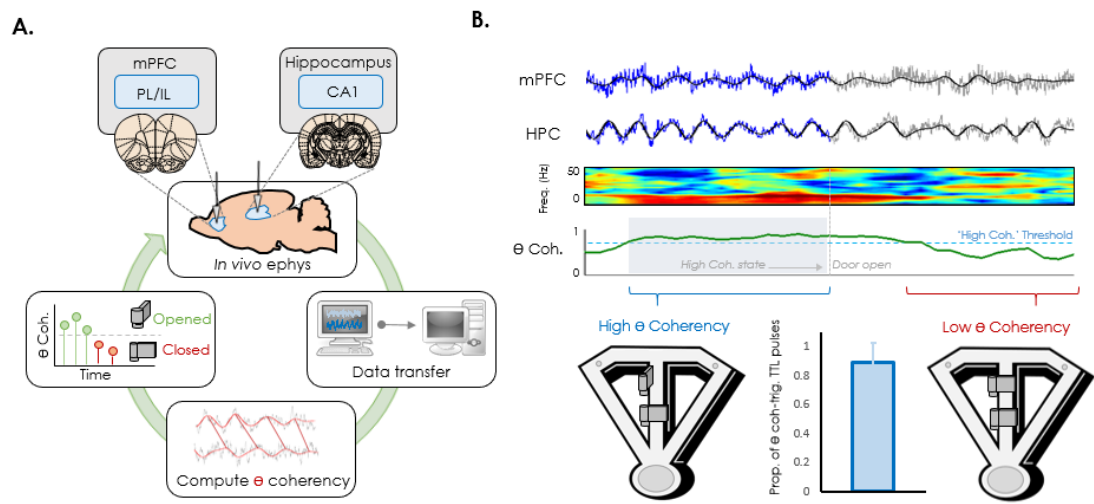


Figure 3 Utilizing endogenous HPC-mPFC theta synchrony. (A) Schematic depicting the closed-loop to be used for initiating memory task trials based upon detection of high HPC-mPFC theta coherence states. LFPs will be simultaneously recorded from HPC and mPFC and routed to another computer to analyze for theta coherence, and if high theta coherence is detected, then a TTL pulse will be sent to initiate the opening of an automated door on the T-maze. (B) Top rows, raw LFP traces from mPFC and HPC with filtered theta overlaid showing high theta coherence in blue. Middle rows, coherogram depicts high theta coherence represented via the warmer colors toward the theta range (4-12 Hz), with the line plot showing high coherence specific to the theta frequency range. This example detection of a high theta coherence state would initiate a command to send a TTL pulse that would be used to open a door on the maze and initiate a memory task trial for the rat to perform (bottom left). However, if HPC-mPFC theta coherence remains low and does not exceed the high coherence threshold, then the door will remain closed (bottom right). Bottom middle, the current loop successfully detects high theta coherence states 89% of the time; however, this will likely increase to 100% with supplemental programming of the Hardware Processing Platform (HPP) to be used in tandem with our digital recording system (Digital Lynx, Neuralynx) to fully support low-latency feedback stimulation.

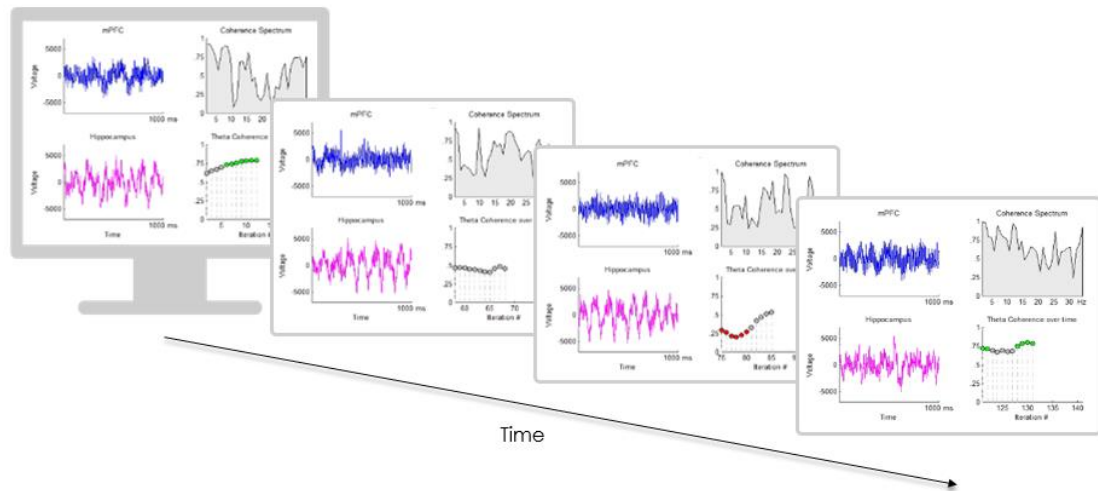


Figure 4 Schematic of the closed-loop for detecting high HPC-mPFC theta coherence in real-time. Upper left panel on screen depicts mPFC LFP (blue), bottom left panel depicts HPC LFP (magenta), top right panel depicts wideband coherence spectrum, and bottom right depicts coherence specific to the theta frequency band. Note the dynamic tracking of HPC-mPFC theta coherence in the bottom right portion of the screen with green and red signaling high and low levels of theta coherence.

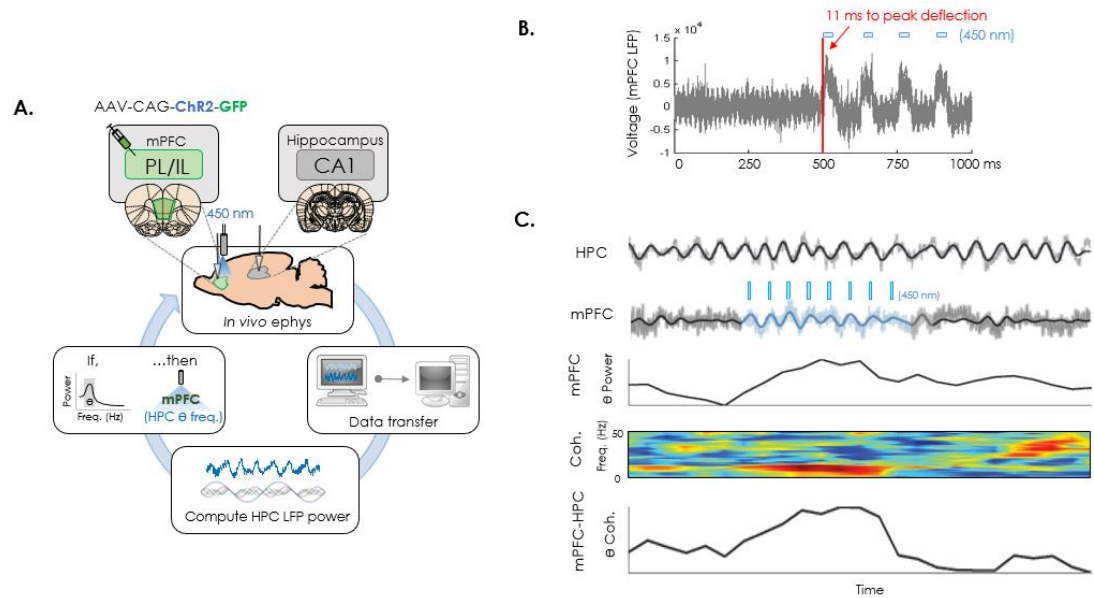


Figure 5 Exogenously driving theta activity in mPFC. (A) Schematic depicting the closed-loop for inducing theta rhythmicity in mPFC via detected theta activity in HPC. First, a viral vector containing Channelrhodopsin is injected into mPFC to transduce neurons with an excitatory opsin. Subsequently, electrodes are placed in HPC and mPFC with an optic fiber positioned over mPFC to activate the transduced neurons with blue light (450 nm). Operation of the closed-loop will record LFP activity from HPC and route it to another computer which will analyze for theta power, and if HPC is in a theta state, then blue light pulses will be emitted over mPFC at the HPC theta frequency to facilitate HPC-mPFC theta synchrony. LFP activity from mPFC will be recorded and later analyzed offline. (B) From the time the blue light pulse is emitted, the induced excitation is observed in the LFP with a peak deflection occurring at an 11 millisecond latency (grey lines depict multiple LFP traces from multiple theta stimulation trains overlaid). (C) Top rows, raw LFPs (grey) with filtered theta overlaid (black), with induced theta rhythmicity in mPFC via a 1-second 8-Hz stimulation train (blue). Bottom rows, blue light theta pulses in mPFC increase mPFC theta power, and increase HPC-mPFC theta coherence depicted in the coherogram, with warmer colors indicating higher coherence in the theta frequency range, and in the line plot below depicting theta frequency band-specific coherence.

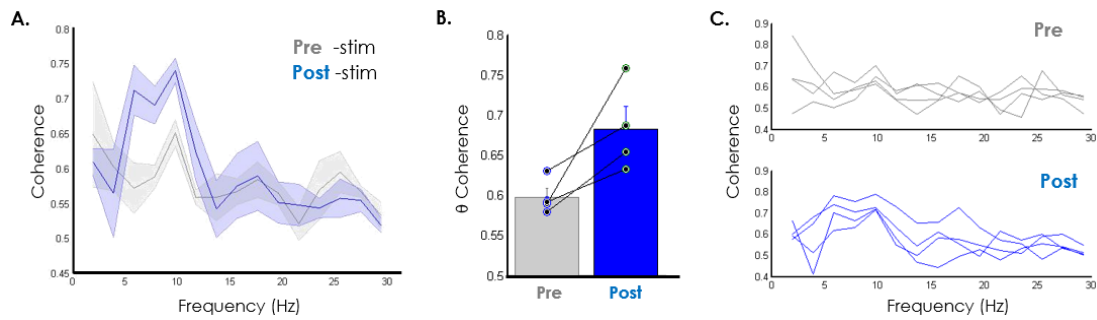


Figure 6 Exogenously inducing theta rhythmicity in mPFC increases HPC-mPFC theta coherence. (A) Blue light pulses delivered at the theta frequency increases phase coherence between HPC and mPFC in the theta frequency range (5-12 Hz) (pre-stim, grey; post-stim, blue, $n = 4$ rats). (B) Theta band-specific coherence is higher during blue light stimulation (mean \pm sem: pre: $.59 \pm .01$, post: $.68 \pm .3$; Kolmogorov-Smirnov test, $p = .0111$, $n = 4$ rats). (C) Individual coherence plots for each rat for pre- and post-stimulation.

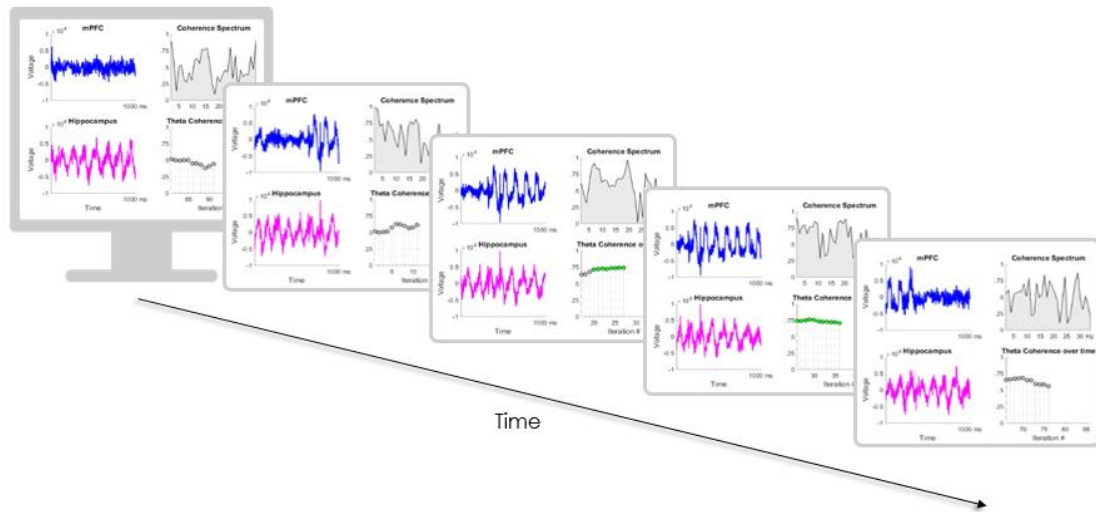


Figure 7 **Schematic of inducing theta rhythmicity and increasing HPC-mPFC theta coherence in real-time.** Upper left panel on screen depicts mPFC LFP (blue), bottom left panel depicts HPC LFP (magenta), top right panel depicts wideband coherence spectrum, and bottom right depicts coherence specific to the theta frequency band. Note the induced theta rhythm in mPFC (blue) during blue light theta frequency pulsing in the bottom left, and the increase in HPC-mPFC coherence in the bottom right.

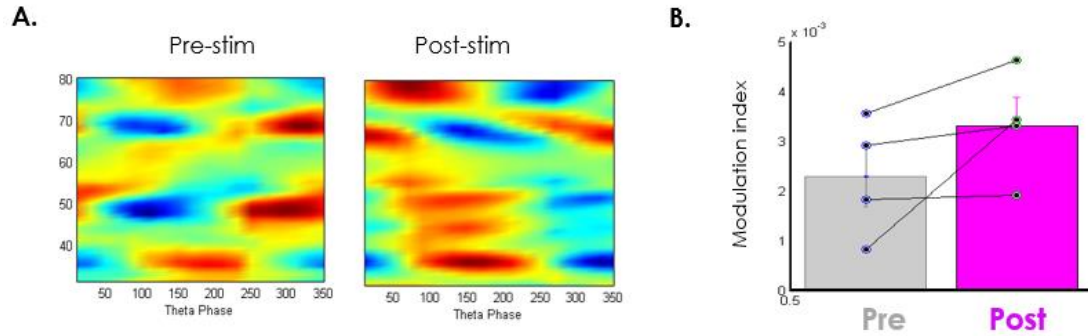


Figure 8 **Theta pulsing in mPFC increases theta-gamma coupling.** (A) Heat maps showing higher coupling of gamma amplitude to theta phase in mPFC during blue light stimulation as depicted via warmer colors toward the center of the theta cycle phase range in the post-stim compared to the pre-stim. (B) Quantifying the degree of theta phase-gamma amplitude coupling shows increased coupling with blue light pulsing (pre: $.0023 \pm .00062$, post: $.0033 \pm .00056$; Kolmogorov-Smirnov test, $p > .05$, $n = 4$ rats).

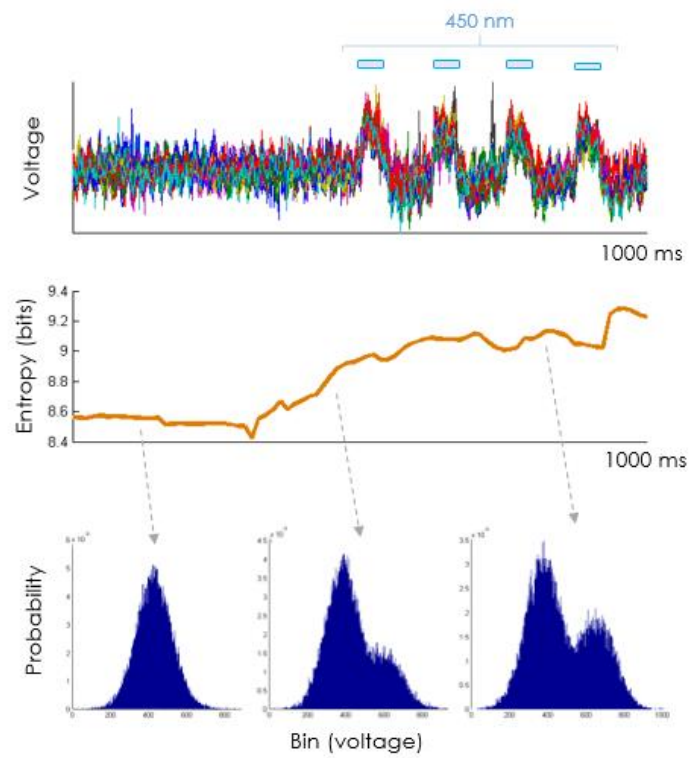


Figure 9 **Blue light pulsing increases information entropy.** Note the change in the probability distributions in the bottom row, as higher entropy indicates the amount of ‘information’ contained in the LFP, as indexed by the probability that an LFP value will fall within a particular voltage bin.

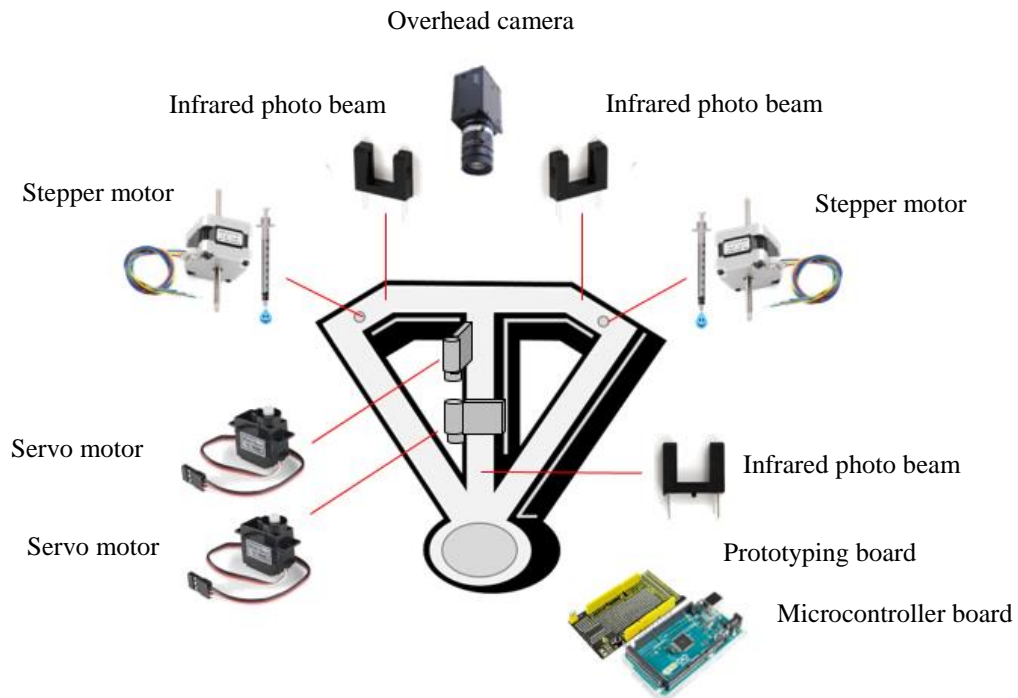


Figure 10 Schematic for automated T-maze. A combination of motors and infrared beam detectors will be programmed with an Arduino microcontroller, used in conjunction with an overhead camera for spatial tracking, to interface with the closed-loops to control trial start times and blue light pulsing. A microcontroller board attached to a prototyping board will be used to configure and control input-out relations to what is programmed in the microcontroller. The prototyping board will be designed to interface the microcontroller with the motors and sensors positioned on the maze. Two servo motors will be used to control the doors that will be used to confine the rat to the start box zone on the maze. Three sets of photo beams will be used to detect when the rat has entered specific zones (i.e., left/right reward zones and start box zone). Two stepper motors will be used to dispel liquid reward in the reward zones and each will be powered by a motor driver.

REFERENCES

- Abbas, A., Sundiang, M., Henoch, B., Morton, M., Bolkan, S., Park, A., Harris, A., Kellendonk, C., & Gordon, J. (2018). Somatostatin interneurons facilitate hippocampal-prefrontal synchrony and prefrontal spatial encoding. *Neuron*, 100, 926-939.
- Adey, W., Dunlop, C., & Hendrix, C. (1960). Hippocampal slow waves: Distribution and phase relations in the course of approach learning. *Archiv Neurology*, 3, 74-90.
- Aghajan, Z., Schuette, P., Fields, T., Tran, M., Siddiqui, S., Hasulak, N., Tcheng, T., Eliashiv, D., Stern, J., Fried, I., & Suthana, N. (2017). Theta oscillations in the human medial temporal lobe during real world ambulatory movement. *bioRxiv*
- Allen, T., Salz, D., McKenzie, S., & Fortin, N. (2016). Nonspatial sequence coding in CA neurons. *J Neuro*, 36, 5, 1547-1563.
- Amit, R., Abeles, D., Bar-Gad, I., & Yuval-Greenberg, S. (2017). Temporal dynamics of saccades explained by a self-paced process. *Scientific Reports*, 7, 886.
- Aronov, D., Nevers, R., & Tank, D. Mapping of a non-spatial dimension by the hippocampal-entorhinal circuit. *Nature*, 719-722.
- Barry, C., Bush, D., O'Keefe, J., & Burgess, N. (2012). Models of grid cells and theta oscillations. *Nature*, 488.
- Bastos, A., Vezoli, J., Bosman, C., Schoffelen, J., Oostenveld, R., Dowdall, J., De Weerd, P., Kennedy, H., & Fries, P. (2015). Visual areas exert feedforward and feedback influences through distinct frequency channels. *Neuron*, 85, 2, 390-401.
- Benchenane, K., Peyrache, A., Khamassi, M., Tierney, P., Gioanni, Y., Battaglia, F., & Wiener, S. (2010). Coherent theta oscillations and reorganization of spike

- timing in the hippocampal-prefrontal network upon learning. *Neuron* 66(6), 921-936.
- Berry, S., & Thompson, R. (1978). Prediction of learning rate from the hippocampal electroencephalogram. *Science*, 200, 4347, 1298-1300.
- Bland, B. (1986). The physiology and pharmacology of hippocampal formation theta rhythms. *Prog Neurobio*, 26, 1-54.
- Bland, B., & Oddie, S. (2001). Theta band oscillation and synchrony in the hippocampal formation and associated structures: The case for its role in sensorimotor integration. *Behav Brain Research*, 127, 119-136.
- Bohbot, V., Copara, M., Gotman, J., & Ekstrom, A. (2017). Low-frequency theta oscillations in the human hippocampus during real-world and virtual navigation. *Nat Comm*
- Bolkan, S., Stujenske, J., Parnaudeau, S., Spellman, T., Rauffenbart, C., Abbas, A., Harris, A., Gordon, J., & Kellendonk, C. (2017). Thalamic projections sustain prefrontal activity during working memory maintenance. *Nature Neuroscience*, 20, 987-996.
- Brandon, M., Bogaard, A., Libby, C., Connerney, M., Gupta, K., & Hasselmo, M. (2011). Reduction of theta rhythm dissociates grid cell spatial periodicity from directional tuning. *Science*, 332, 6029, 595-599.
- Brown, B. (1968). Frequency and phase of hippocampal theta activity in the spontaneously behaving cat. *Electroenceph & Clin Neurophysiol*, 24, 1, 53-62.
- Burke, J. F., Merkow, M. B., Jacobs, J., Kahana, M. J., & Zaghoul, K. A. (2015). Brain computer interface to enhance episodic memory in human participants. *Frontiers in Human Neuro*, 8, 1055.
- Buzsáki, G. (2002). Theta oscillations in the hippocampus. *Neuron*, 33, 325-340.
- Buzsáki, G. (2006). *Rhythms of the Brain*. New York: Oxford University Press.
- Buzsaki, G. (2010). Neural syntax: Cell assemblies, synapsesembles, and readers. *Neuron*, 68, 362-385.

- Buzsáki, G. Anastassiou, C. A., & Koch, C. (2012). The origin of extracellular fields and currents: EEG, ECoG, LFP, and spikes. *Nature Rev Neurosci*, 13, 407-420.
- Buzsaki, G., & Tingley, D. (2018). Space and time: The hippocampus as a sequence generator. *Trends in Cogn Sci*, 22, 10, 853-869.
- Churchwell, J. C., Morris, A. M., Mussco, N. D., & Kesner, R. P. (2010). Prefrontal and hippocampal contributions to encoding and retrieval of spatial memory. *Neurobiol Learn Mem*, 93, 415-421.
- Climer, J., DiTullio, R., Newman, E., Hasselmo, M., & Eden, U. (2015). Examination of rhythmicity of extracellularly recorded neurons in the entorhinal cortex. *Hippocampus*, 25, 4, 460-473.
- Cohen, M. X. (2014). *Analyzing neural time series data*. Cambridge, Massachusetts: MIT Press.
- Cole, S., & Voytek, B. (2018). Cycle-by-cycle analysis of neural oscillations. *bioRxiv*
- Colgin, L., Denninger, T., Fyhn, M., Hafting, T., Bonnevie, T. Jensen, O., Moser, M., & Moser, E. (2009). Frequency of gamma oscillations routes flow of information in the hippocampus. *Nature*, 462, 7271, 353-357.
- Colgin, L. (2011). Oscillations and hippocampal-prefrontal synchrony. *Curr Opin in Neuribio*, 21, 467-474.
- Danjo, T., Toyozumi, T., & Fujisawa, S. (2018). Spatial representations of self and other in the hippocampus. *Science*, 359, 6372, 213-218.
- Ekstrom, A., Kahana, M., Caplan, J., Fields, T., Isham, E., Newman, E., & Fried, I. (2003). Cellular networks underlying human spatial navigation. *Nature*, 425, 184-187.
- Ekstrom, A., Caplan, J., Ho, E., Shattuck, K., Fried, I., & Kahana, M. (2005). Human hippocampal theta activity during virtual navigation. *Hippocampus*, 15, 881-889.

- Eliav, T., Geva-Sagiv, M., Yartsev, M., Finkelstein, A., Rubin, A., Las, L., & Ulanovsky, N. (2018). Nonoscillatory phase coding and synchronization in the bat hippocampal formation. *Cell*, 175, 4, 1119-1130.
- Fell, J., & Axmacher, N. (2011). The role of phase synchronization in memory processes. *Nature Reviews Neuroscience*, 12, 105–118. <http://doi.org/10.1038/nrn2979>
- Floresco, S. B., Seamans, J. K., & Phillips, A. G. (1997). Selective roles for hippocampal, prefrontal cortical, and ventral striatal circuits in radial-arm maze tasks with or without a delay. *J Neuro*, 17, 1880-1890.
- Forslid, A., Andersson, B., & Johansson, S. (1986). Observations on normal EEG activity in different brain regions of the unrestrained swine. *Acta Physiol Scand*, 128, 3, 389-396.
- Fujisawa, S., & Buzsaki, G. (2011). A 4-Hz oscillation adaptively synchronizes prefrontal, VTA and hippocampal activities. *Neuron*, 72, 1, 153-165.
- Gordon, J. (2011). Oscillations and hippocampal-prefrontal synchrony. *Curr Opin in Neurobio*, 21, 486-491.
- Goyal, A., Miller, J., Qasim, S., Watrous, A., Stein, J., Inman, C., Gross, R., Willie, J., Lega, B., Lin, J., Sharan, A., Wu, C., Sperling, M., Sheth, S., McKhann, G., Smith, E., Schevon, C., & Jacobs, J. (2018). Functionally distinct high and low theta oscillations in the human hippocampus. *bioRxiv*
- Graystan, E., Lissak, K., Madarsz, I., Donhoffer, H. (1959). Hippocampal electrical activity during the development of conditioned reflexes. *Electroencephalograph Clin Neurophysiol*, 11, 409-430.
- Green, J., & Arduini. (1954). Hippocampal electrical activity in arousal. *J Neurophysiol*, 17, 6, 533-557.
- Griffin, A., Asaka, Y., Darling, R., & Berry, S. (2004). Theta-contingent trial presentation accelerates learning rate and enhances hippocampal plasticity during trace eyeblink conditioning. *Learn Mem*, 11, 604-610.

- Griffin, A., & Hallock, H. (2013). Hippocampal signatures of episodic memory: Evidence from single-unit recording studies. *Frontiers in Behav Neurosci*
- Grion, N., Akrami, A., Zuo, Y., Stella, F., & Diamond, E. (2016). Coherence between rat sensorimotor system and hippocampus is enhanced during tactile discrimination. *PLoS Biol*, 14, 2.
- Guise, K., & Shapiro, M. (2017). Medial prefrontal cortex reduces memory interference by modifying hippocampal encoding. *Neuron*, 94, 1, 183-192.
- Hallock, H. L., & Griffin, A. L. (2013). Dynamic coding of dorsal hippocampal neurons between tasks that differ in structure and memory demand. *Hippocampus*, 23, 169-186.
- Hallock, H. L., Arreoal, A. C., Shaw, C. L., & Griffin, A. L. (2013a). Dissociable roles of the dorsal striatum and dorsal hippocampus in conditional discrimination and spatial alternation T-maze tasks. *Neurobiol Learn Memory*, 100, 108-116.
- Hallock, H. L., Wang, A., Shaw, C. L., & Griffin, A. L. (2013b). Transient inactivation of the thalamic nucleus reuniens and rhomboid nucleus produces deficits of a working-memory dependent tactile-visual conditional discrimination task. *Behav Neurosci*, 127(6), 860–866.
- Hallock, H. L., Wang, A., & Griffin, A. L. (2016). Ventral midline thalamus is critical for hippocampal-prefrontal synchrony and spatial working memory. *The Journal of Neuroscience*, 36(32), 8372–89.
- Hasselmo, M., Bodelon, C., & Wyble, B. (2002). A proposed function for hippocampal theta rhythm: Separate phases for encoding and retrieval. *Neural Comput*, 14, 4, 793-817.
- Heys, J., MacLeod, K., Moss, C., & Hasselmo, M. (2013). Bat and rat neurons differ in theta-frequency resonance despite similar coding of space. *Science*, 340, 6130, 363-367.
- Hoffman, K., Dragan, M., Leonard, T., Micheli, C., Montefusco-Siegmund, R., & Valiante, T. (2013). Saccades during visual exploration align hippocampal 3-8 Hz rhythms in human and non-human primates. *Frontiers Syst Neuro*, 7, 43.

- Hyman, J., Wyble, B., Goyal, V., Rossi, C., & Hasselmo, M. (2003). Stimulation in hippocampal region CA1 in behaving rats yields long-term potentiation when delivered to the peak of theta and long-term depression when delivered to the trough. *J Neuro*, 23, 37, 11725-11731.
- Hyman, J. M., Zilli, E. A., Paley, A. M., & Hasselmo, M. E. (2010). Working memory performance correlates with prefrontal-hippocampal theta interactions but not with prefrontal neuron firing rates. *Frontiers in Integrative Neuroscience*, 4(2), 1–13.
- Griffin, A., Asaka, Y., Darling, R., & Berry, S. (2004). Theta-contingent trial presentation accelerates learning rate and enhances hippocampal plasticity during trace eyeblink conditioning. *Behav Neuro*, 118, 2, 403-411.
- Jarovi, J., Volle, J., Yu, X., Guan, L., & Takehara-Nishiuchi, K. (2018). Prefrontal theta oscillations promote selective encoding of behaviorally relevant events. *eNeuro*, 5, 6, 1-16.
- Jones, M. W., & Wilson, M. A. (2005). Theta rhythms coordinate hippocampal-prefrontal interactions in a spatial memory task. *PLoS BIOLOGY*, 3(12), 2187–2199.
- Jung, R., & Kornmuller, A. (1938). Eine methodic der ableitun lokalisierter potential schwankingen aus subcorticalen hirnyebieten. *Arch Psychiat Neruenkr*, 109, 1-30.
- Jung, M., Wiener, S., & McNaughton, B. (1994). Comparison of spatial firing characteristics of units in dorsal and ventral hippocampus of the rat. *J Neuro*, 14, 12, 7347-7356.
- Jutras, M., & Buffalo, E. (2010). Synchronous neural activity and memory formation. *Curr Opin Neurobiol*, 20, 2, 150-155.
- Jutras, M., & Buffalo, E. (2013). Oscillatory activity in the monkey hippocampus during visual exploration and memory formation. *PNAS*, 110, 32, 13144-13149.

- Jutras, M., & Buffalo, E. (2014). Oscillatory correlates of memory in non-human primates. *NeuroImage*, 85, 694-701.
- Killian, N., Jutras, M., & Buffalo, E. (2012). A map of visual space in the primate entorhinal cortex. *Nature*, 491, 7426, 761-764.
- Kitchigina, V. (2018). Alterations of theta and gamma network oscillations as an early biomarker of temporal lobe epilepsy and Alzheimer's disease. *Front Integr Neurosci*, 12, 36.
- Kjelstrup, K., Solstad, T., Brun, V., Hafting, T., Leutgeb, S., Witter, M., Moser, E., & Moser, M. (2008). Finite scale of spatial representation in the hippocampus. *Science*, 321, 5885, 140-143.
- Kramer, R., Vanderwolf, C., & Bland, B. (1975). Two types of hippocampal rhythmical slow activity in both the rabbit and the rat: Relations to behavior and effects of atropine, diethyl ether, urethane, and pentobarbital. *Exp Neurology*, 49, 1, 1, 58-85.
- Landfield, P., McGaugh, J., & Tusa, R. (1972). Theta rhythm: a temporal correlate of memory storage processes in the rat. *Science*, 175, 87-89.
- Leonard, T., Mikkila, J., Eskandar, E., Gerrard, J., Kaping, D., Patel, S., Wolmelsdorf, T., & Hoffman, K. (2015). Sharp wave ripples during visual exploration in the primate hippocampus. *J Neuro*, 35, 44, 14771-14782.
- Leonard, T., & Hoffman, K. (2017). Sharp-wave ripples in primates are enhanced near remembered visual objects. *Current Biol*, 27, 257-262.
- Lisman, J. E., & Jensen, O. (2013). The theta-gamma neural code. *Neuron*, 77(6), 1002–1016.
- Lubenov, E., & Siapas, A. (2009). Hippocampal theta oscillations are travelling waves. *Nature*, 459, 534-539.
- Macrides, F. (1975). Temporal relationships between hippocampal slow waves and exploratory sniffing in hamsters. *Behavioral Biology*, 14, 295-308.



- Maisson, D., & Gemzik, Z., & Griffin, A. (2018). Optogenetic suppression of the nucleus reuniens selectively impairs encoding during spatial working memory. *Neurobio Learn Mem*, 155, 78-85.
- Mankin, E., Thurley, K., Chenani, A., Haas, O., Debs, L., Henke, J., Galinato, M., Leutgeb, J., Leutgeb, S., & Leibold, C. (2019). The hippocampal code for space in Mongolian gerbil. *Hippocampus*
- Miller, J., Neufang, M., Solway, A., Brandt, A., Trippel, M., Mader, I., Hefft, S., Merkow, M., Polyn, S., Jacobs, J., Kahana, M., & Schulze-Bonhage, A. (2013). Neural activity in human hippocampal formation reveals the spatial context of retrieved memories. *Science*, 342, 1111-1114.
- Mitra, P., & Bokil, H. (2008). *Observed Brain Dynamics*. New York: Oxford University Press.
- Myroshenchenko, M., Seamans, J. K., Phillips, A. G., & Lapish, C. C. (2017). Temporal dynamics of hippocampal and medial prefrontal cortex interactions during the delay period of a working memory-guided foraging task. *Cereb Cortex*, 27, 11, 5331-5342.
- Newman, E., Gillet, S., Climer, J., & Hasselmo, M. (2013). Cholinergic blockade reduces theta-gamma phase amplitude coupling and speed modulation of theta frequency consistent with behavioral effects on encoding. *J Neuro*, 33, 50, 19635-19646.
- O'Neill, P. K., Gordon, J. A., & Sigurdsson, T. (2013). Theta oscillations in the medial prefrontal cortex are modulated by spatial working memory and synchronize with the hippocampus through its ventral subregion. *The Journal of Neuroscience*, 33(35), 14211-24.
- Patel, J., Fujisawa, S., Berenyi, A., Royer, S., & Buzsaki, G. (2012). Traveling theta waves along the entire septo-temporal axis of the hippocampus. *Neuron*, 75, 3, 410-417.
- Place, R., Farovik, A., Brockman, M., & Eichenbaum, H. (2016). Bidirectional prefrontal-hippocampal interactions support context-guided memory.

- Robinson, T. (1980). Hippocampal rhythmic slow activity (RSA, theta): a critical analysis of selected studies and discussion of possible-species differences. *Brain Res Rev*, 2, 69-101.
- Royer, S., Sirota, A., Patel, J., & Buzsaki, G. (2010). Distinct representations and theta dynamics in dorsal and ventral hippocampus. *J Neuro*, 30, 5, 1777-1787.
- Saalman, Y. B. (2014). Intralaminar and medial thalamic influence on cortical synchrony, information transmission and cognition. *Frontiers in Systems Neuroscience*, 8(83), 1–8. <http://doi.org/10.3389/fnsys.2014.00083>
- Seager, M., Johnson, L., Chabot, E., Asaka, Y., & Berry, S. (2002). Oscillatory brain states and learning: Impact of hippocampal theta-contingent training. *PNAS*, 99, 3, 1616-1620.
- Schmidt, B., Hinman, J., Jacobson, T., Szkudlarek, E., Argraves, M., Escabi, M., & Markus, E. (2013). Dissociation between dorsal and ventral hippocampal theta oscillations during decision-making. *J Neuro*, 33, 14, 6212-6224.
- Schomburg, E., G, Fernandez-Ruiz, A., Mizuseki, K., Berenyi, A., Anastassiou, C., Koch, C., & Buzsaki, G. (2014). Theta phase segregation of input-specific gamma patterns in entorhinal-hippocampal networks. *Neuron*, 84, 2, 470-485.
- Shannon, C. (1948). A mathematical theory of communication. *Bell System Tech Journal*, 27, 3, 379-423.
- Siapas, A. G., Lubenov, E. V., & Wilson, M. A. (2005). Prefrontal phase locking to hippocampal theta oscillations. *Neuron* 46, 1, 141-151.
- Siegel, J., Nitz, D., & Bingman, V. (2000). Hippocampal theta rhythm in awake, freely moving homing pigeons. *Hippocampus*, 10, 627-631.
- Siegle, J., & Wilson, M. (2014). Enhancement of encoding and retrieval functions through theta-phase specific manipulations of hippocampus. *eLife*
- Spellman, T., Rigotti, M., Ahmari, S. E., Fusi, S., Gogos, J. A., & Gordon, J. A. (2015). Hippocampal-prefrontal input supports spatial encoding in working memory. *Nature*, 522(7556), 309–14.

- Tamura, M., Mukai, J., Gordon, J., & Gogos, J. (2016). Developmental inhibition of Gsk3 rescues behavioral and neurophysiological deficits in a mouse model of schizophrenia predisposition. *Neuron*, 89, 1100-1109.
- Tamura, M., Spellman, T. J., Rosen, A. M., Gogos, J. A., & Gordon, J. A. (2017). Hippocampal-prefrontal theta-gamma coupling during performance of a spatial working memory task. *Nature Comm*, 8, 2182
- Tingley, D., & Buzsaki, G. (2018). Transformation of a spatial map across the hippocampal-lateral septal circuit. *Neuron*, 98, 6, 1229-1242.
- Ulanovksy, N., & Moss, C. (2007). Hippocampal cellular and network activity in freely moving echolocating bats. *Nature Neuro*, 10, 2, 224-233.
- Ulanovksy, N., & Moss, C. (2011). Dynamics of hippocampal spatial representation in echolocating bats. *Hippocampus*, 21, 2, 150-161.
- Vanderwolf, C. (1969). Hippocampal electrical activity and voluntary movement in the rat. *Electroencephalogy Clin Neurophysiol*, 26, 407-418.
- Watrous, A., Lee, D. Izadi, A., Gurkoff, G., Shahlaie, K., & Ekstrom, A. (2013). A comparative study of human and rat hippocampal low-frequency oscillations during spatial navigation. *Hippocampus*, 23, 8, 656-661.
- Winson, J. (1972). Interspecies differences in the occurrence of theta. *Behav Biol*, 7, 4, 479-487.
- Yartsev, M., Witter, M., & Ulanovsky, N. (2011). Grid cells without theta oscillations in the entorhinal cortex of bats. *Nature*, 479, 103-107.
- Yartsev, M., & Ulanovsky, N. (2013). Representation of three-dimensional space in the hippocampus of flying bats. *Science*, 340, 6130, 367-372.
- Zhang, H., & Jacobs, J. (2015). Traveling theta waves in the human hippocampus. *J Neuro*, 35, 36, 12477-12487.
- Zhang, H., Watrous, A., Patel, A., & Jacobs, J. (2015). Theta and alpha oscillations are travelling waves in the human neocortex. *J Neuro*, 35, 36, 12477-12487.

Appendix A

ANIMAL PROTOCOL PERMISSION

	Office of Laboratory Animal Medicine	Life Science Research Facility 79 E. Delaware Avenue Newark, DE 19711 Phone: 302-831-2616 Fax: 302-831-0154
<p>To: Office of Graduate and Professional Education</p>		
<p>From: Gwen Talham, DVM, Director, Animal Care Program </p>		
<p>Subject: IACUC approval for Andrew Garcia</p>		
<p>Date: 4/8/2019</p>		
<p>Andrew Garcia was approved by the IACUC to work with animals on Amy Griffin's protocol #1177 "Neural Correlates of Spatial and Nonspatial Memory". Please contact me at 831-2980 or gtalham@udel.edu with any additional questions.</p>		
<hr/>		
<p>www.udel.edu</p>		